Improved Noise Propagation in Statistical Image Reconstruction with Resolution Modeling

Arman Rahmim[1], Ju-Chieh Cheng[2], and Vesna Sossi[2]
[1]Department of Radiology, Johns Hopkins University School of Medicine, Baltimore, MD 21205
[2]Department of Physics and Astronomy, University of British Columbia, Vancouver, BC V6T 1Z1
E-mail: arahmim1@jhmi.edu, jcheng@phas.ubc.ca, and vesna@phas.ubc.ca

***Abstract*— Positron emission tomography (PET), like other imaging modalities, has resolution limitations. Two general/common approaches to improve reconstructed image resolution include: (i) the de-convolution scheme, and (ii) system matrix modeling (in statistical image reconstruction methods). An interesting observation about (ii) is that it is able to improve both resolution and noise characteristics of the reconstructed images (unlike (i) which offers a trade-off). In this work, we have used the unified noise model developed by Qi [5] to perform image covariance calculations without and with the inclusion of resolution modeling in the system matrix of the EM algorithm. We have in particular shown that, while system matrix modeling of finite resolution effects improves the image resolution by direct contribution to the reconstruction task, it is at the same time able to lower the reconstructed image noise due to a compression/widening effect in inter-voxel correlations. We have also experimentally verified this effect.**

I. Introduction

Resolution limitations in positron emission tomography (PET) are caused/determined by positron range, photon non-collinearity, detector size and inter-crystal scattering/penetration effects. Two general approaches have been used in order to address the reconstructed image resolution:

(i) De-convolution scheme: This technique is established by noting that the reconstructed image of a point source can be modeled as the convolution of the point source with the point spread function (PSF), referred to as the system transfer function (STF) in the Fourier domain. It then follows from the convolution theorem that the imaged object, in the Fourier domain, can be obtained via division of the reconstructed image, in the Fourier domain, by the STF. The important limitation of this technique is that while increasing the imaging frequency, it results in high-frequency noise amplification.

(ii) System Matrix Modeling: One of the key motivations behind the wide-spread use of statistical image reconstruction techniques has been the ability to incorporate more accurate modeling of system response in the PET acquisition process. To see how this technique works, we note that, for a J-dimensional image vector and an I-dimensional projection set, the system matrix P=$(p_{ij})_{I\times J}$ may be decomposed as [1], [2]: $P = WGB$, where, the matrix B=$(b_{ij})_{J\times J}$ is introduced to account for the aforementioned finite resolution effects, while the matrices G=$(g_{ij})_{I\times J}$ and W=$(w_{ij})_{I\times I}$ contain the geometric and sensitivity (attenuation and normalization) effects, respectively. An interesting observation about this latter technique is that it is able to improve *both* resolution *and* noise characteristics of the reconstructed images. We investigate in this work as to how and why this is achieved.

It must be noted here that as compared to the aforementioned *purely* image-space based modeling of resolution effects, used in this work, a more accurate approach involves the modeling of the photon non-collinearity and detector effects in the G and/or W matrices instead, as is done in [3], [4]. Improvements in noise propagation using these approaches will be investigated in the future.

II. Noise Analysis

Denoting the sensitivity factor at a voxel j by $\varsigma_j = \sum_{i=1}^{I} p_{ij}$, and using $\vec{\varsigma}$ and $\vec{\lambda}^m$ as J-dimensional vectors of voxel sensitivity and image intensity, the EM algorithm can be written in the following way:

$$\lambda^{\vec{m+1}} = \frac{\vec{\lambda^m}}{\vec{\varsigma}} \times P' \left\{ \frac{\vec{y}}{P\vec{\lambda^m}} \right\} \quad (1)$$

where $\vec{y}$ is the measured data set, while neglecting randoms and scattered events for now. We then write:

$$\vec{\lambda^m} = \vec{\bar{\lambda}^m} + \vec{\epsilon^m} \quad (2)$$

$$\vec{y} = \vec{\bar{y}} + \vec{\delta} \quad (3)$$

where $\vec{\bar{\lambda}^m}$ denotes the expected image over all noisy realizations of the mean data $\vec{\bar{y}}$ (and therefore, $\vec{\epsilon^m}$ and $\vec{\delta}$ are zero-mean noise vectors for the image and data, respectively). At iteration m, the image covariance matrix C_ϵ^m is given by $C_\epsilon^m = V^m C_\delta [V^m]'$, where C_δ is the covariance matrix for the data (modeled in this work using independent Poisson statistics; i.e. $C_\delta = \text{diag}[\vec{\bar{y}}]$), and V_m is a $J \times I$ matrix relating data noise to image noise; i.e. $\vec{\epsilon^m} = V^m \vec{\delta}$.

In Ref. [5], Qi has developed a nicely unified noise model applicable to a wide range of iterative image estimation techniques. For the EM scheme, this can be written as:

$$V_\epsilon^{m+1} = [I - A^m]V^m + B^m \quad \text{where} \quad V^{m=0} = 0 \quad (4)$$

$$B^m = \text{diag}[\frac{\vec{\bar{\lambda}^m}}{\vec{\varsigma}}] P' \text{diag}[P\vec{\bar{\lambda}^m}]^{-1} \quad (5)$$

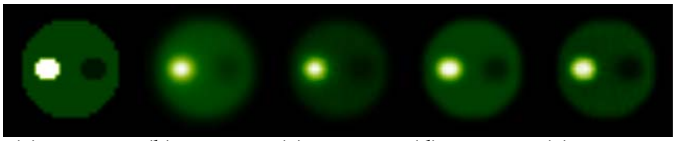

(a) (b) (c) (d) (e)

Fig. 1. (a) The phantom image. (b) mean and (c) variance images after iteration 5. (d) mean and (e) variance images after iteration 25.

$$A^m = \text{diag}[\frac{\vec{\bar{\lambda}^m}}{\vec{\varsigma}}]P'\text{diag}[P\vec{\bar{\lambda}^m}]^{-2}\text{diag}[\vec{y}]P - \text{diag}[\frac{\vec{\bar{\lambda}^{m+1}}}{\vec{\bar{\lambda}^m}}] + I \tag{6}$$

In the classical treatment by Barrett *et al.* [6], the authors have made the approximation that the projection of the mean reconstructed image at iteration m is equal to the noise-free data (i.e. $P\vec{\bar{\lambda}^m} \sim \vec{y}$, which implies also that $\vec{\bar{\lambda}^{m+1}} \sim \vec{\bar{\lambda}^m}$), from which it follows that:

$$A^m = \text{diag}[\frac{\vec{\bar{\lambda}^m}}{\vec{\varsigma}}]P'\text{diag}[P\vec{\bar{\lambda}^m}]^{-1}P \tag{7}$$

However, as we demonstrate next, this approximation is indeed non-negligible. Furthermore, we have investigated properties of the covariance images obtained without and with the system matrix resolution modeling technique.

A. Noise Matrix Calculations

We performed calculations in the 2D case to further investigate properties of resolution modeling in the EM algorithm. Two computer phantoms were considered: (i) a contrast disc with cold (activity 1/3 of background) and hot (activity 4 times background) regions, and (ii) a uniform disc. The phantoms were represented using 32x32 square pixels. The sinogram had 32 projection angles covering 180° and 32 detector bins per angle with a sampling distance of one pixel, and a Gaussian resolution blurring with FWHM of 2.0 pixels. Scattered and random events were not simulated in this work.

Fig. 1 shows the original contrast phantom image, as well as the reconstructed mean and variance images (with resolution modeling) after 5 and 25 iterations. It is interestingly noted [6] that the variance images appear proportional compared to the mean image. This is in fact an advantage of statistical EM reconstruction over analytic techniques, since low activity regions also exhibit low variance levels, thus not overly 'contaminated' by more active regions (in contrast with FBP-like reconstruction schemes).

To compare the analytical results derived in [5] and [6], we have considered both Eqs. (6) and (7) in the noise propagation calculations. Fig. 2a compares the resulting variance estimates in the hot, cold and background regions for the two derivations. Clear inconsistencies are observed. To explain them, we note that the mean values in the three regions, as depicted in Fig. 2b, converge in different direction. That is, in early iterations, $\bar{\lambda}_j^{m+1}/\bar{\lambda}_j^m > 1$ for all voxels j in the hot region, $\bar{\lambda}_j^{m+1}/\bar{\lambda}_j^m \sim 1$ for the background region, and $\bar{\lambda}_j^{m+1}/\bar{\lambda}_j^m < 1$ for the cold region. Subsequently, the term $\text{diag}[\vec{\bar{\lambda}^{m+1}}/\vec{\bar{\lambda}^m}]$ in (6) (neglected in (7)) accounts for

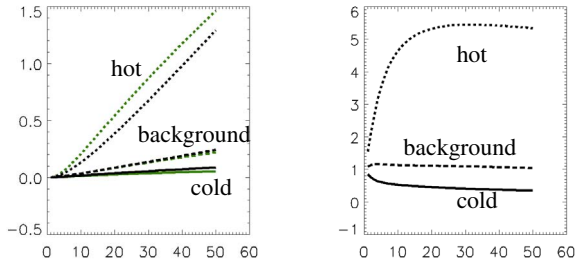

(a) (b)

Fig. 2. (a) Calculated variance plots for the hot (dotted), background (− −), and cold (solid) regions using Eq. 6 (black) vs. Eq. 7 (green). (b) Mean plots for the three regions.

underestimated and overestimated variance values for the hot and cold regions, respectively, when using the aforementioned additional approximation leading to (7). Furthermore, we have observed the incorrect noise calculations to carry themselves over to subsequent, later iterations. As a consequence, in this work, we have used the more accurate expression (6).

B. Image Covariance Comparisons

Fig. 3(a) shows a typical covariance image for a particular voxel in the uniform disc. It is seen that the degree of correlation diminishes for increasingly distant voxels. Comparing the resulting covariance values for reconstructions without and with resolution modeling, it is typically observed (Figs. 3b,c), that the latter scheme reduces the variance value (peak of the covariance curve) while increasing the width of the correlation curve. This can be intuitively attributed to the fact that the blurring operation in the system matrix (during the projection steps) results in an increased level of inter-correlation amongst nearby voxels. This has direct implications with regards to measurements of spatial variance (discussed in next part). Furthermore, we note that resolution modeling reduces the 'amount of negative correlations' which may be seen to reduce large oscillations within a ROI (this aspect will be explored in later work).

We next note that modeling of resolution effects into the system matrix implies that an improved image resolution is expected, which combined with the aforementioned increase in inter-voxel correlations, explain the simultaneous improvements in image resolution *and* noise properties. This is in contrast to de-convolution techniques, which do *not* contribute to the reconstruction task itself, and subsequently only result in trade-offs between resolution and noise.

C. Relation of the Covariance Matrix to Spatial Variance

We note that, for a profile through a region S of the reconstructed image $\vec{\lambda}$, the spatial variance σ_s^2 has an expectation given by:

$$\langle \sigma_s^2 \rangle = \frac{n}{n-1}\left\langle \frac{1}{n}\sum_{j\in S}\lambda_j^2 - \left(\frac{1}{n}\sum_{j\in S}\lambda_j\right)^2 \right\rangle \tag{8}$$

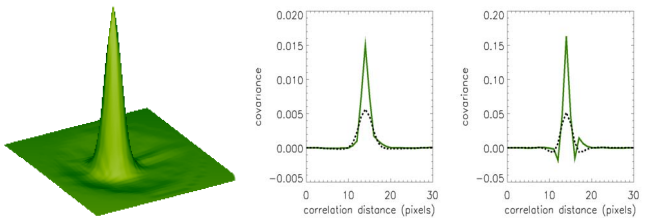

(a) (b) (c)

Fig. 3. (a) A typical covariance image for a particular voxel. 1D axial profiles through the covariance image for reconstructions without (solid) and with (dotted) resolution modeling after 5 (b) and 25 (c) iterations.

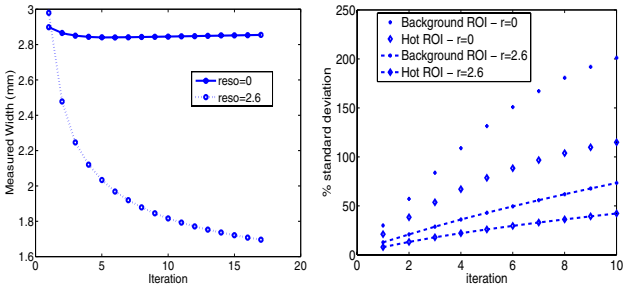

(a) (b)

Fig. 4. Plots of (a) reconstructed FWHM and (b) percentage noise vs. iteration without (r=0) and with (r=2.6 mm) resolution modeling.

where $\langle . \rangle$ denotes an average over the ensemble of noisy data. Then:

$$\langle \sigma_s^2 \rangle = \frac{1}{n-1} \sum_j \langle \lambda_j^2 \rangle - \frac{1}{n(n-1)} \left(\sum_j \langle \lambda_j^2 \rangle + \sum_{j \neq k} \langle \lambda_j \lambda_m \rangle \right) \quad (9)$$

As an example, we next note that for a simplified model of a uniform reconstructed region such that (i) all voxels have equal mean and variance, and (ii) with any voxel j there are p voxels which are fully correlated (i.e. $\langle \lambda_j \lambda_l \rangle = \langle \lambda^2 \rangle$) while the other voxels are not correlated at all (i.e. $\langle \lambda_j \lambda_l \rangle = \langle \lambda \rangle^2$), it then follows that:

$$\langle \sigma_s^2 \rangle = \frac{n}{n-1} \langle \lambda^2 \rangle - \frac{1}{n-1} \langle \lambda^2 \rangle - \frac{p}{n-1} \langle \lambda^2 \rangle - \frac{(n-1)-p}{n-1} \langle \lambda \rangle^2 \quad (10)$$

$$\langle \sigma_s^2 \rangle = \frac{n-1-p}{n-1} \left(\langle \lambda^2 \rangle - \langle \lambda \rangle^2 \right) = \left(1 - \frac{p}{n-1} \right) \sigma_v^2 \quad (11)$$

where σ_v^2 is the individual voxel variance. Comparing the reconstruction schemes without and with resolution modeling, we note that in the latter, at a given iteration, σ_v^2 is relatively smaller while the inter-voxel effective correlation width (i.e. p in the simplified model) is larger, thus predicting a smaller spatial variance for voxels in a uniform region, as we also demonstrate experimentally next.

III. Experiment – Phantom Studies

Tomograph: Data were acquired on the second generation of the high resolution research tomographs (HRRT). This HRRT scanner has an octagonal design, with the detector heads consisting of a double 10 mm layer of LSO/LYSO for a total of 119,808 detector crystals (crystal size 2.1 x 2.1 x 10 mm^3).

Experiment 1 – Printed Point Source: Using a technique that allows printing of radioactive point sources using a modified standard ink-jet printer, we imaged a radioactive (^{18}F) point source of size 0.7 mm placed 3 cm radially away from the center of the FOV.

Experiment 2 – Contrast Phantom: A 20 cm long, 10 cm radius phantom was used. The phantom had a 5 cm diameter cylindrical insert filled with a ^{11}C radioactivity concentration of 59.4 kBq/ml ('hot' insert). The phantom itself was filled with a ^{18}C concentration of 11.5 kBq/ml ('background'), yielding a hot insert to background ratio of 5.2. The total counts in the frame were 32 M.

Implementation: The resolution modeling technique is applicable to both histogram-mode and list-mode image reconstruction techniques. In the context of state-of-the-art PET imaging, the latter has been our reconstruction scheme of choice (implementation of the list-mode reconstruction scheme on the HRRT scanner has been elaborated in [7]).

Results: Figs. 4(a,b) show plots of (a) resolution and (b) percentage noise (measured on a voxel-basis in a ROI) as functions of EM iterations without resolution modeling as well as with the use of a 2.6 mm Gaussian kernel to perform resolution modeling. Clearly the EM reconstruction algorithm is able to improve the reconstructed FWHM *as well as* the noise properties upon inclusion of resolution modeling, as we have predicted using noise propagation calculations. Future work will focus on various types of noise measurements (voxel-based, ROI-based, etc.).

IV. Conclusion

In this work, we have used the unified noise model developed by Qi [5] to perform image covariance calculations without and with the inclusion of finite resolution modeling in the system matrix of the EM algorithm. We have, in particular, shown that while the technique improves the image resolution by direct contribution to the reconstruction task (unlike the de-convolution technique), it is at the same time able to lower the reconstructed image noise due to a compression/widening effect in the covariance curves for the image voxels. We have also experimentally verified this effect.

References

[1] E. Mumcuoğlu *et al.*, *IEEE Trans. Med. Imag.*, vol. 13, pp. 687, 1994.
[2] A. J. Reader *et al.*, *IEEE Trans. Nucl. Sci.* vol. 49, pp. 693-699, 2002.
[3] E. Ü. Mumcuoğlu, et al., *IEEE Nucl. Sci. Symp. Conf. Record.*, vol. 3, 1569-1573, 1996.
[4] R. M. Leahy and J. Qi, *Stat. Comput.*, vol. 10, pp. 147-165, 2000.
[5] J. Qi, *Phys. Med. Biol.*, vol. 48, pp. 3505-3519, 2003.
[6] H. H. Barrett *et al.*, *Phys. Med. Biol.*, vol. 39, pp. 833-846, 1994.
[7] A. Rahmim *et al.*, *Phys. Med. Biol.*, vol. 49, pp. 4239-4258, 2004.